

MIT Open Access Articles

*Synthesis, Characterization, and Cytotoxicity
of Platinum(IV) Carbamate Complexes*

The MIT Faculty has made this article openly available. **Please share** how this access benefits you. Your story matters.

Citation: Wilson, Justin J., and Stephen J. Lippard. "Synthesis, Characterization, and Cytotoxicity of Platinum(IV) Carbamate Complexes." *Inorganic Chemistry* 50.7 (2011): 3103–3115. Web.

As Published: <http://dx.doi.org/10.1021/ic2000816>

Publisher: American Chemical Society

Persistent URL: <http://hdl.handle.net/1721.1/71116>

Version: Author's final manuscript: final author's manuscript post peer review, without publisher's formatting or copy editing

Terms of Use: Article is made available in accordance with the publisher's policy and may be subject to US copyright law. Please refer to the publisher's site for terms of use.



Synthesis, Characterization, and Cytotoxicity of Platinum(IV) Carbamate Complexes

*Justin J. Wilson and Stephen J. Lippard**

Department of Chemistry, Massachusetts Institute of Technology, Cambridge, MA 02139

lippard@mit.edu

RECEIVED DATE (to be automatically inserted after your manuscript is accepted if required according to the journal that you are submitting your paper to)

The synthesis, characterization, and cytotoxicity of eight new platinum(IV) complexes having the general formula, c,c,t -[Pt(NH₃)₂Cl₂(O₂CNHR)₂], are reported, where R = *tert*-butyl (**4**), cyclopentyl (**5**), cyclohexyl (**6**), phenyl (**7**), *p*-tolyl (**8**), *p*-anisole (**9**), 4-fluorophenyl (**10**), or 1-naphthyl (**11**). These compounds were synthesized by reacting organic isocyanates with the platinum(IV) complex, c,c,t -[Pt(NH₃)₂Cl₂(OH)₂]. The electrochemistry of the compounds was investigated by cyclic voltammetry. The aryl carbamate complexes **7** – **11** exhibit reduction peak potentials near -720 mV vs. Ag/AgCl, whereas the alkyl carbamate complexes display reduction peak potentials between -820 and -850 mV vs. Ag/AgCl. The cyclic voltammograms of c,c,t -[Pt(NH₃)₂Cl₂(O₂CCH₃)₂] (**1**), c,c,t -[Pt(NH₃)₂Cl₂(O₂CCF₃)₂] (**2**), and *cis*-[Pt(NH₃)₂Cl₄] (**3**) were measured for comparison. Density functional theory (DFT) studies were undertaken to investi-

gate the electronic structures of **1** – **11** and to determine their adiabatic electron affinities. A linear correlation ($R^2 = 0.887$) between computed adiabatic electron affinities and measured reduction peak potential was discovered. The biological activity of **4** – **11** and, for comparison, cisplatin was evaluated in human lung cancer A549 and normal MRC-5 cells by the MTT assay. The compounds exhibit comparable or slightly better activity than cisplatin against the A549 cells. In MRC-5 cells, all are equally or slightly less cytotoxic than cisplatin, except for **4** and **5**, which are more toxic.

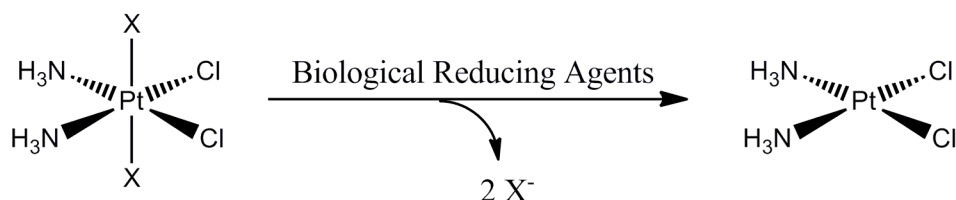
Introduction

The simple coordination compound, *cis*-diamminedichloroplatinum(II) or cisplatin, is an effective anticancer drug that has been used in the clinic since 1978.¹ Its success has given rise to the second-generation platinum drugs, carboplatin and oxaliplatin. These three platinum(II) complexes are believed to operate by a similar mechanism. Aquation of the leaving groups, chloride for cisplatin, carboxylate and oxalate for carboplatin and oxaliplatin, respectively, generates reactive *cis*-diam(m)ineplatinum cations, which react readily with the purine nucleobases in DNA.^{2,3} Structural distortions in DNA induced by platinum binding⁴⁻⁷ trigger multiple cellular responses that ultimately lead to cell death.^{8,9}

Despite the clinical success of these compounds, the requirement for intravenous administration and associated long-term toxic side effects¹⁰⁻¹² diminish the quality of life for patients. Platinum anticancer complexes in the +4 oxidation state have shown considerable promise for both oral administration and for reducing systematic toxicity.¹³⁻¹⁵ The orally administered platinum(IV) complex, satraplatin, progressed as far as Phase III in clinical trials.¹⁶ The increased stability of these complexes, due to their low-spin d^6 electronic configuration, aids in their survival of the acidic environment of the stomach before being absorbed into the bloodstream. They operate by a mechanism similar to that of the first and second generation

operate by a mechanism similar to that of the first and second generation platinum(II) analogues. An activation step, namely reduction from Pt(IV) to Pt(II), must occur before aquation and DNA binding, however (Scheme 1).

Scheme 1.



In addition to their kinetic stability, another favorable property of platinum(IV) complexes relative to their platinum(II) counterparts is the presence of two additional coordination sites that can be modified to alter their pharmacokinetic properties. By varying the two axial ligands, one can predictably alter the redox potential¹⁷⁻¹⁹ and lipophilicity²⁰⁻²² of the platinum(IV) complex while leaving the DNA binding *cis*-diammineplatinum moiety unaltered. Furthermore, the axial coordination sites can serve as binding sites for other biologically active ligands, which may have synergistic effects with platinum therapy, as demonstrated by us²³⁻²⁵ and by others.^{26, 27} The ability to tether platinum(IV) complexes via the axial ligands to various nano-delivery devices for increased cellular uptake and selectivity²⁸⁻³⁵ is another advantage. The design of new platinum(IV) anticancer complexes, however, is limited by the current synthetic methodology.³⁶⁻⁴² Most of the newly tested platinum(IV) complexes bear either chloro, hydroxo, or carboxylato axial ligands. The development of new synthetic methodologies for accessing the platinum(IV) manifold can expand the range of complexes having novel properties.

The synthesis of platinum(IV) complexes with axial methyl, ethyl, and isopropyl carbamate ligands was described over 10 years ago.³⁶ Since then, their biological properties have only rarely been explored,⁴³ and further investigations of the scope of this synthetic methodology have

not been pursued. In the present work, we report both a modification and expansion of this approach through the synthesis of eight new platinum(IV) complexes of both alkyl and aryl carbamates as well as a brief investigation of their biological activity. Computational DFT studies were undertaken to gain a deeper understanding of the electronic structure of these new complexes. The results presented here indicate that platinum(IV) carbamates are a promising new class of potential anticancer agents.

Experimental

General Considerations. All reactions were carried out under normal atmospheric conditions. Solvents were used as received without additional drying or purification. All isocyanates were used as received from commercial vendors. The compounds *c,c,t*-[Pt(NH₃)₂Cl₂(OH)₂], *c,c,t*-[Pt(NH₃)₂Cl₂(O₂CCH₃)₂] (**1**), and *c*-[Pt(NH₃)₂Cl₄] (**3**) were synthesized as previously described^{44,45} using cisplatin purchased from Strem Chemicals, Inc. as the starting material.

Physical Measurements. NMR measurements were recorded on a Bruker DPX-400 spectrometer in the MIT Department of Chemistry Instrumentation Facility at 20 °C with deuterated dimethylsulfoxide (DMSO-*d*₆) as the solvent. All NMR chemical shifts (δ) are reported in parts per million (ppm) and referenced as described below. ¹H and ¹³C{¹H} NMR spectra were referenced internally to residual solvent peaks and chemical shifts are expressed relative to tetramethylsilane, SiMe₄ (δ = 0 ppm). ¹⁹⁵Pt{¹H} and ¹⁹F{¹H} NMR spectra and were referenced externally using standards of K₂PtCl₄ in D₂O (δ = -1628 ppm) and trifluorotoluene (δ = -63.72 ppm), respectively. Fourier transform infrared (FTIR) spectra were recorded with a ThermoNicolet Avatar 360 spectrophotometer running the OMNIC software. Samples were prepared as KBr disks. Cyclic voltammograms were obtained at room temperature using a VersaSTAT3 potentiostat from

Princeton Applied Research accompanied by the V3 Studio software. A three electrode system was used comprising a glassy carbon electrode as the working electrode, a Pt wire as the auxiliary electrode, and Ag/AgCl (aqueous, saturated NaCl) electrode as the reference electrode. Samples were prepared as 2 mM solutions in *N,N*-dimethylformamide (DMF) with 0.1 M (*n*-Bu₄N)PF₆ as the supporting electrolyte. Reported values are peak potentials of the irreversible reduction event at a scan rate of 100 mV/s. Under the conditions described here, the reversible ferrocene/ferrocenium redox couple was consistently found between 0.54 – 0.55 V vs. Ag/AgCl. Electrospray ionization mass spectrometry (ESI-MS) measurements were acquired on an Agilent Technologies 1100 series LC-MSD trap.

Synthesis of *c,c,t*-[Pt(NH₃)₂Cl₂(O₂CCF₃)₂] (2**).** The compound *c,c,t*-[Pt(NH₃)₂Cl₂(OH)₂] (0.144 g, 0.429 mmol) was suspended in 2 mL of trifluoroacetic anhydride. The mixture was stirred for 1 h at room temperature, open to air, at which point the volatile anhydride had evaporated, leaving a white residue. A 2 mL volume of tetrahydrofuran (THF) was added to the residue, and the resulting yellow solution was filtered through Celite. Pentane (~10 mL) was layered on top of the THF solution and the mixture was kept at -40 °C for 1 h to afford pale yellow microcrystals of **2**. These microcrystals were collected by vacuum filtration and washed with pentane before being dried in vacuo. Yield: 0.127 g (56%). ¹H NMR (400 MHz): δ 6.63 (br s, 6H). ¹³C{¹H} NMR (100 MHz): δ 161.8 (q, ²J_{CF} = 37 Hz), 111.7 (q, ¹J_{CF} = 288 Hz). ¹⁹F{¹H} NMR (377 MHz): δ -73.6. ¹⁹⁵Pt{¹H} NMR (86 MHz): δ 1182. IR (KBr, cm⁻¹): 3426 m br, 3280 s, 3232 s, 3197 s, 3075 m, 1722 vs, 1559 w, 1382 m, 1331 m, 1212 s, 1162 vs, 1034 w, 859 w, 781 m, 739 m, 524 w. Anal. Calcd. for **2**, C₄H₆Cl₂F₆N₂O₄Pt: C, 9.13; H, 1.15; N, 5.32. Found: C, 9.38; H, 1.21; N, 5.31.

General Synthesis of *c,c,t*-[Pt(NH₃)₂Cl₂(O₂CNHR)₂]. To a suspension of *c,c,t*-[Pt(NH₃)₂Cl₂(OH)₂] (0.20 g, 0.60 mmol) in 1 mL of DMF was added a 1 mL DMF solution con-

taining 4 mol-equiv of the isocyanate. The resulting mixture was stirred for 12 h at room temperature, resulting in the formation of a homogenous solution. The solution was filtered and the desired product was precipitated by the addition of diethyl ether. The solid was collected by either filtration or centrifugation. To remove residual DMF, the solid was suspended in water for 30 min, isolated by centrifugation, resuspended in ethanol, isolated by centrifugation, resuspended in diethyl ether, isolated by centrifugation, and finally dried under vacuum.

Compound 4. R = *tert*-butyl. White solid. Yield: 0.153 g (48%). Mp 238–245 °C (dec). ^1H NMR (400 MHz): δ 6.65 (br, 6H), 6.05 (br, 2H), 1.17 (s, 18H). $^{13}\text{C}\{^1\text{H}\}$ NMR 100 MHz): δ 162.8, 49.4, 29.3. $^{195}\text{Pt}\{^1\text{H}\}$ NMR (86 MHz): δ 1276. IR (KBr, cm^{-1}): 3387 vs, 3301 m, 3220 s, 2975 m, 2931 w, 1640 vs, 1629 vs, 1505 vs, 1462 m, 1393 w, 1366 m, 1281 vs, 1211 s, 1079 m, 943 m, 788 w, 727 w, 645 w, 569 w, 434 w. ESI-MS (neg. ion mode): m/z 531.1 [M]. Anal. Calcd. for **4**, $\text{C}_{10}\text{H}_{26}\text{Cl}_2\text{N}_4\text{O}_4\text{Pt}$: C, 22.56; H, 4.92; N, 10.52. Found: C, 23.14; H, 4.83; N, 10.65.

Compound 5. R = cyclopentyl. White solid. Yield: 0.240 g (72%). Mp 208–214 °C (dec). ^1H NMR (400 MHz): δ 6.67 (br, 6H), 6.55 (br, 2H), 3.78 – 3.71 (m, 2H), 1.68 – 1.34 (m, 16H). $^{13}\text{C}\{^1\text{H}\}$ NMR (400 MHz): δ 163.4, 52.7, 32.5, 23.3. $^{195}\text{Pt}\{^1\text{H}\}$ NMR (86 MHz): δ 1274 (major), 1262 (minor). IR (KBr, cm^{-1}): 3402 s, 3354 vs, 3243 vs, 2959 s, 2869 m, 1629 vs, 1509 vs, 1358 m, 1297 s, 1252 s, 1099 w, 1037 w, 1008 w, 953 w, 782 w, 581 w. ESI-MS (neg. ion mode): m/z 555.0 [M]. Anal. Calcd. for **5**, $\text{C}_{12}\text{H}_{26}\text{Cl}_2\text{N}_4\text{O}_4\text{Pt}$: C, 25.91; H, 4.71; N, 10.07. Found: C, 25.76; H, 4.66; N, 10.29.

Compound 6. R = cyclohexyl. White solid. Yield: 0.287 g (81%). Mp 228–233 °C (dec). ^1H NMR (400 MHz): δ 6.67 (br, 6H), 6.47 (br, 2H), 3.19 (br, 2H), 1.71 – 1.50 (m, 10H), 1.22 – 1.02 (m, 10H). $^{13}\text{C}\{^1\text{H}\}$ NMR (100 MHz): δ 163.0, 50.0, 33.1, 25.3, 24.9. $^{195}\text{Pt}\{^1\text{H}\}$ NMR (86 MHz): δ 1276 (major), 1263 (minor). IR (KBr, cm^{-1}): 3375 vs, 3304 m, 3239 s, 2931 s, 2853 m, 1628

vs, 1500 vs, 1244 s, 1035 m, 931 w, 783 w, 724 w, 706 w, 587 w. ESI-MS (neg. ion mode): m/z 583.0 $[M - H]^-$. Anal. Calcd. for **6**, $C_{14}H_{30}Cl_2N_4O_4Pt$: C, 28.77; H, 5.17; N, 9.59. Found: C, 28.89; H, 5.20; N, 9.44.

Compound 7. R = phenyl. Yellow solid. Yield: 0.214 g (60%). Mp 171–176 °C (dec). 1H NMR (400 MHz): δ 9.12 (br, 2H), 7.47 (d, 4H), 7.18 (t, 4H), 6.86 (t, 2H), 6.79 (br, 6H). $^{13}C\{^1H\}$ NMR (100 MHz): δ 160.7, 140.7, 128.3, 121.0, 118.0. $^{195}Pt\{^1H\}$ NMR (86 MHz): δ 1265. IR (KBr, cm^{-1}): 3243 s br, 1654 vs, 1595 s, 1514 s, 1438 s, 1393 s, 1315 s, 1227 s, 1045 m, 1025 m, 754 m, 691 m. ESI-MS (neg. ion mode): m/z 570.9 $[M - H]^-$. Anal. Calcd. for **7**, $C_{14}H_{18}Cl_2N_4O_4Pt$: C, 29.38; H, 3.17; N, 9.79. Found: C, 29.56; H, 3.07; N, 9.67.

Compound 8. R = *para*-tolyl. Pale orange solid. Yield: 0.229 g (64%). Mp 149–151 °C (dec). 1H NMR (400 MHz): δ 9.02 (br, 2H), 7.36 (d, 4H), 6.98 (d, 4H), 6.79 (br, 6H), 2.20 (s, 6H). $^{13}C\{^1H\}$ NMR (100 MHz): δ 160.8, 138.2, 129.7, 128.7, 118.1, 20.4. $^{195}Pt\{^1H\}$ NMR (86 MHz): δ 1264. IR (KBr, cm^{-1}): 3404 s, 3353 s, 3217 br vs, 2924 w, 1663 vs, 1635 s, 1592 m, 1522 vs, 1502 m, 1404 m, 1314 s, 1289 s, 1250 m, 1223 vs, 1041 s, 817 m, 776 m, 740 w, 654 w, 582 w, 510 w. ESI-MS (neg. ion mode): m/z 599.0 $[M - H]^-$, 1199.0 $[2M - H]^-$. Anal. Calcd. for **8**, $C_{16}H_{22}Cl_2N_4O_4Pt$: C, 32.01; H, 3.69; N, 9.31. Found: C, 32.14; H, 3.75; N, 9.51.

Compound 9. R = *para*-anisole. Pale orange solid. Yield: 0.190 g (50%). Mp 115–117 °C (dec). 1H NMR (400 MHz): δ 8.98 (br, 2H), 7.37 (d, 4H), 6.77 (br d, 10H), 3.68 (s, 6H). $^{13}C\{^1H\}$ NMR (100 MHz): δ 160.9, 153.8, 134.0, 119.5, 113.5, 55.1. $^{195}Pt\{^1H\}$ NMR (86 MHz): δ 1265. IR (KBr, cm^{-1}): 3223 s br, 2835 w, 1647 vs, 1515 vs, 1410 m, 1298 s, 1223 vs, 1178 m, 1029 s, 827 m, 777 w, 739 w, 652 m, 583 w, 527 w. ESI-MS (neg. ion mode): m/z 630.9 $[M]^-$. Anal. Calcd. for **9**, $C_{16}H_{22}Cl_2N_4O_4Pt$: C, 30.39; H, 3.51; N, 8.86. Found: C, 30.45; H, 3.48; N, 8.73.

Compound 10. R = 4-fluorophenyl. Pale yellow solid. Yield: 0.237 g (65%). Mp 208–210 °C (dec). ^1H NMR (400 MHz): δ 9.21 (br, 2H), 7.48 – 7.45 (m, 4H), 7.02 (app t, 4H), 6.78 (br, 6H). $^{13}\text{C}\{^1\text{H}\}$ NMR (100 MHz): δ 160.7, 156.9 (d, $^1J_{\text{CF}} = 236$ Hz), 137.1, 119.5, 114.7 (d, $^2J_{\text{CF}} = 22.0$ Hz). $^{19}\text{F}\{^1\text{H}\}$ NMR (377 MHz): δ -125.2 (s, 2F). $^{195}\text{Pt}\{^1\text{H}\}$ NMR (86 MHz): δ 1265. IR (KBr, cm^{-1}): 3367 s, 3238 s br, 1657 vs, 1512 vs, 1407 s, 1389 m, 1305 m, 1259 s, 1213 vs, 1157 w, 1101 w, 1037 s, 832 s, 653 m, 584 w, 513 w. ESI-MS (neg. ion mode): m/z 606.9 $[\text{M} - \text{H}]^-$, 1216.0 $[2\text{M} - \text{H}]^-$. Anal. Calcd. for **10**, $\text{C}_{14}\text{H}_{16}\text{Cl}_2\text{F}_2\text{N}_4\text{O}_4\text{Pt}$: C, 27.64; H, 2.65; N, 9.21. Found: C 27.42; H, 2.50; N, 9.02.

Compound 11. R = 1-naphthyl. Pale orange solid. Yield: 0.093 g (46%, using 0.30 mmol of starting material). Mp 152–157 °C (dec). ^1H NMR (400 MHz): δ 9.01 (s, 2H), 8.19 – 8.17 (m, 2H), 7.88 – 7.85 (m, 2H), 7.67 (d, 2H), 7.62 (d, 2H), 7.50 – 7.40 (m, 6H), 6.82 (br, 6H). $^{13}\text{C}\{^1\text{H}\}$ NMR (100 MHz): δ 161.9, 135.5, 133.7, 127.9, 127.5, 125.7, 125.6, 125.2, 123.5, 123.4, 120.6. $^{195}\text{Pt}\{^1\text{H}\}$ NMR (86 MHz): δ 1269. IR (KBr, cm^{-1}): 3407 (s), 3355 (s), 3211 (s, br), 3063 (m), 1654 (vs), 1566 (m), 1490 (s), 1410 (s), 1341 (s), 1247 (s), 1101 (w), 999 (w), 791 (m), 772 (s), 544 (w). ESI-MS (neg. ion mode): m/z 669.8 $[\text{M} - \text{H}]^-$. Anal. Calcd. for **11**, $\text{C}_{22}\text{H}_{22}\text{Cl}_2\text{N}_4\text{O}_4\text{Pt}$: C, 39.30; H, 3.30; N, 8.33. Found: C, 39.44; H, 3.29; N, 8.39.

X-ray Crystallographic Studies. Single crystals were mounted in Paratone oil on a cryoloop and frozen under a 110 K or 100 K KRYO-FLEX nitrogen cold stream. Data were collected on a Bruker APEX CCD X-ray diffractometer with graphite-monochromated Mo- $\text{K}\alpha$ radiation ($\lambda = 0.71073$ Å) controlled by the APEX2 software package.⁴⁶ Absorption corrections were applied using SADABS.⁴⁷ The structures were solved using direct methods and refined on F^2 with the SHELXTL-97 software package.^{48, 49} Structures were checked for higher symmetry using PLATON.⁵⁰ All non-hydrogen atoms were located and refined anisotropically. Unless otherwise

stated, hydrogen atoms were placed in idealized locations and given isotropic thermal parameters equivalent to either 1.5 (terminal CH₃ or NH₃ hydrogen atoms) or 1.2 times the thermal parameter of the atom to which they were attached. Structure refinement was carried out using established strategies.⁵¹ Specific details regarding crystal growth and refinement are described in the Supporting Information (SI), and parameters are shown in Tables 1, 2, and S1. Selected bond lengths and angles for **2** are listed in Table S2.

Theoretical Calculations. DFT calculations were performed using the Gaussian 03 (Rev.D01) software package.⁵² Geometry optimizations, frequency calculations, and molecular orbital generations were all carried out using the B3LYP functional.^{53,54} For the light atoms (carbon, hydrogen, chlorine, nitrogen, oxygen, and fluorine), the 6-31++G(d,p) basis set⁵⁵ was used, and for platinum, the LANL2DZ basis set and effective core potential⁵⁶ was used. No solvation models were employed; the results described for all complexes are in the gas phase. Frequency calculations were carried out on all optimized geometries to verify the absence of imaginary values. To determine adiabatic electron affinities, an additional set of geometry optimizations and energy calculations were performed for the analogous monoanionic Pt(III) complexes with a doublet spin state. The difference in energy between the Pt(III) anion and neutral Pt(IV) complexes is the adiabatic electron affinity of the latter. The geometry optimization of the 1-electron reduced analogue of *cis*-[Pt(NH₃)₂Cl₄] gave rise to a structure with an imaginary frequency. Hence, its adiabatic electron affinity was not computed. Atomic coordinates, energies, and lowest frequency of all optimized structures are provided in the SI as Tables S3 – S23.

Cell Lines and Culture Conditions. Human A549 (lung carcinoma) and human MRC-5 (normal lung fibroblasts) were grown as adherent monolayers in growth medium consisting of Dulbecco's Modified Eagle Medium (DMEM) supplemented with 10% fetal bovine serum (FBS)

and 1% penicillin/streptomycin. The cultures were grown in 25 cm² flasks in an incubator at 37 °C with a humidified atmosphere composed of 5% CO₂.

Cytotoxicity Assays. The colorimetric MTT assay was used to determine the cytotoxicity of cisplatin and compounds **1** – **6**. Trypsinized A549 and MRC-5 cells were seeded into a 96-well plate at cell densities of 1500 cells/well and 2500 cells/well, respectively, in 200 µL of growth medium and were incubated for 24 h. The medium was then removed, and 200 µL of new growth medium containing various concentrations of the platinum complexes was added. After 72 h, the medium was removed, 200 µL of a 0.8 mg/mL solution of MTT in DMEM was added, and the plate was incubated for an additional 4 h. The DMEM/MTT mixture was aspirated, and 200 µL of dimethylsulfoxide (DMSO) with 10% pH 10.5 glycine buffer were added to dissolve the purple formazan crystals. The absorbance of the plates was read at 570 nm. Absorbance values were normalized to the platinum-free control wells and plotted as [Pt] versus % viability. IC₅₀ values were extrapolated from the resulting curves. The reported IC₅₀ values are the averages from at least three independent experiments, each of which consisted of three replicates per concentration level. Dilutions of the platinum(IV) compounds in growth medium were prepared from concentrated solutions (10 – 20 mM) in DMSO. Cisplatin was diluted from a phosphate-buffered saline solution (2 mM).

Table 1. Summary of the X-Ray Crystallographic Information and Data Collection Parameters for **4** – **7**.

	4 ·3DMSO	5 ·2DMF	6 ·2DMSO	7 ·DMSO·0.5H ₂ O
formula	C ₁₆ H ₄₄ Cl ₂ N ₄ O ₇ PtS ₃	C ₁₈ H ₄₀ Cl ₂ N ₆ O ₆ Pt	C ₁₈ H ₄₂ Cl ₂ N ₄ O ₆ PtS ₂	C ₁₆ H ₂₅ Cl ₂ N ₄ O _{5.5} PtS
fw	766.72	702.55	740.67	659.45
space group	<i>P</i> $\bar{1}$	<i>P</i> $\bar{1}$	<i>Pbcn</i>	<i>P2₁/c</i>
<i>a</i> , Å	8.9361(10)	9.0048(9)	25.5442(17)	11.5530(5)
<i>b</i> , Å	10.5917(12)	12.6877(13)	10.7982(7)	31.3292(13)
<i>c</i> , Å	16.762(2)	13.2385(14)	20.7211(13)	13.5070(6)
α , deg	89.100(2)	116.484(2)		
β , deg	89.454(2)	93.069(2)		109.7380(10)
γ , deg	72.258(2)	92.288(2)		
<i>V</i> , Å ³	1510.8(3)	1348.4(2)	5715.5(6)	4601.6(3)
<i>Z</i>	2	2	8	8
ρ_{calcd} , g·cm ⁻³	1.685	1.730	1.721	1.904
<i>T</i> , °C	-173(2)	-173(2)	-173(2)	-173(2)
$\mu(\text{Mo K}\alpha)$, mm ⁻¹	5.066	5.444	5.281	6.458
Θ range, deg	2.02–28.25	1.72–29.73	1.59–29.18	1.73–25.11
total no. of data	30171	29870	118407	75374
no. of unique data	7386	7585	7718	8189
no. of parameters	337	304	323	546
completeness to Θ (%)	98.9	98.7	100.0	99.8
R1 ^a (%)	2.91	2.38	4.27	3.44
wR2 ^b (%)	5.50	5.00	5.66	4.96
GOF ^c	1.040	1.039	1.021	1.044
max, min peaks, e ⁻ ·Å ⁻³	1.749, -1.229	1.879, -2.044	1.672, -0.787	1.264, -0.733

^aR1 = $\sum |F_o| - |F_c| / \sum |F_o|$. ^bwR2 = $\{\sum [w(F_o^2 - F_c^2)^2] / \sum [w(F_o^2)^2]\}^{1/2}$. ^cGOF = $\{\sum [w(F_o^2 - F_c^2)^2] / (n - p)\}^{1/2}$ where *n* is the number of data and *p* is the number of refined parameters.

Table 2. Summary of the X-Ray Crystallographic Information and Data Collection Parameters for **8** – **11**.

	8 ·2DMSO·0.74H ₂ O	9 ·acetone	10 ·3.5DMF	11 ·3DMF
formula	C ₂₀ H ₃₅ Cl ₂ N ₄ O _{6.74} PtS ₂	C ₁₉ H ₂₈ Cl ₂ N ₄ O ₇ Pt	C _{24.5} H _{40.5} Cl ₂ F ₂ N _{7.5} O _{7.5} Pt	C ₃₁ H ₄₃ Cl ₂ N ₇ O ₇ Pt
fw	769.55	690.44	864.13	891.71
space group	<i>P</i> $\bar{1}$	<i>P</i> 2 ₁ / <i>c</i>	<i>P</i> 2 ₁	<i>P</i> $\bar{1}$
<i>a</i> , Å	11.6514(7)	18.9166(10)	18.0923(7)	11.7178(14)
<i>b</i> , Å	14.7016(8)	9.5089(5)	7.0254(3)	12.0190(15)
<i>c</i> , Å	18.4270(11)	13.7632(7)	26.4980(11)	13.2152(16)
α , deg	68.7800(10)			87.170(2)
β , deg	78.9840(10)	92.5790(10)	104.0310(10)	77.548(2)
γ , deg	84.3020(10)			75.264(2)
<i>V</i> , Å ³	2886.6(3)	2473.2(2)	3267.6(2)	1757.6(4)
<i>Z</i>	4	4	4	2
ρ_{calcd} , g·cm ⁻³	1.771	1.854	1.757	1.685
<i>T</i> , °C	-173(2)	-173(2)	-163(2)	-173(2)
μ (Mo K α), mm ⁻¹	5.234	5.935	4.524	4.199
Θ range, deg	1.49–29.32	2.16–28.74	1.24–28.66	1.58–28.40
total no. of data	60845	51159	68723	35819
no. of unique data	15609	6409	16640	8716
no. of parameters	706	304	903	457
completeness to Θ (%)	98.7	99.7	99.8	98.8
R1 ^a (%)	4.36	2.82	2.83	2.27
wR2 ^b (%)	8.05	4.83	5.70	4.21
GOF ^c	1.029	1.030	1.039	1.037
max, min peaks, e ⁻ Å ⁻³	3.119, -2.625	2.131, -0.468	1.221, -1.191	0.942, -0.712

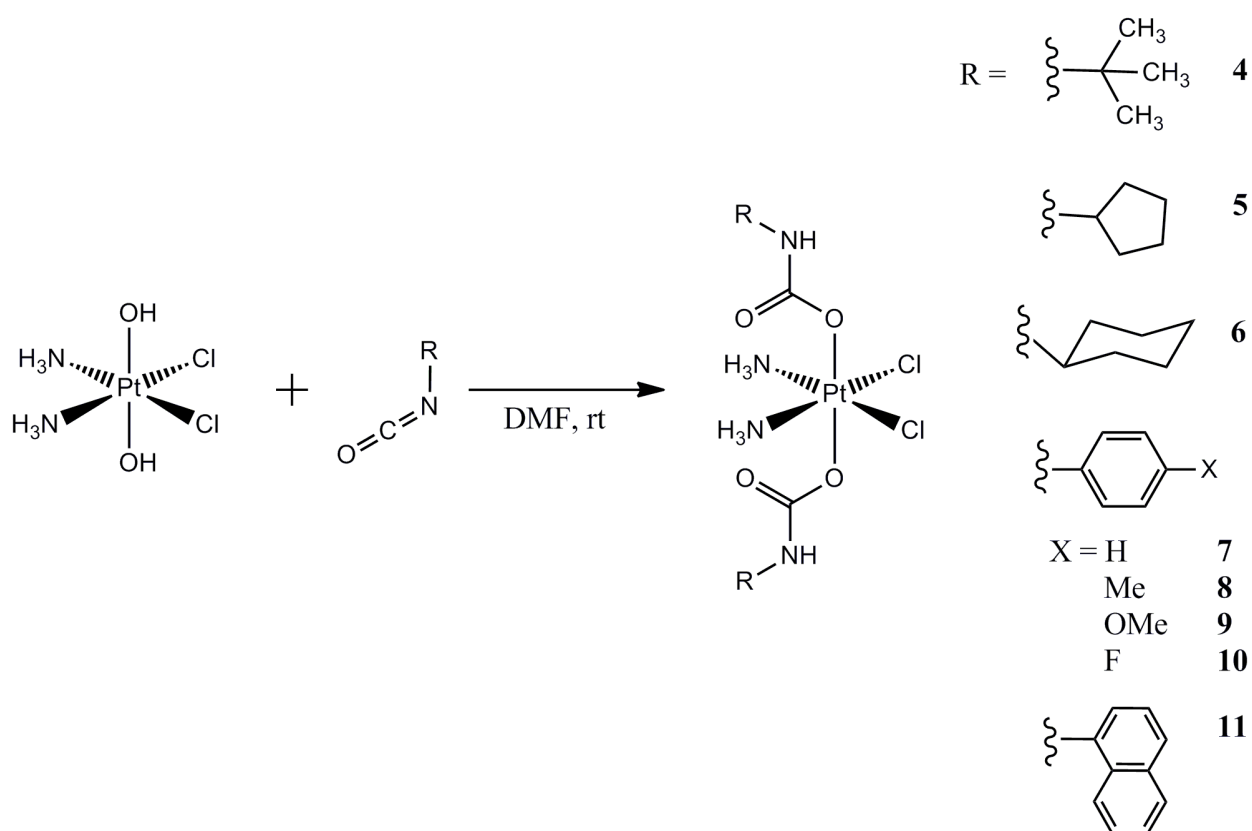
^aR1 = $\sum||F_o| - |F_c|| / \sum|F_o|$. ^bwR2 = $\{\sum[w(F_o^2 - F_c^2)^2] / \sum[w(F_o^2)^2]\}^{1/2}$. ^cGOF = $\{\sum[w(F_o^2 - F_c^2)^2] / (n - p)\}^{1/2}$ where *n* is the number of data and *p* is the number of refined parameters.

Results and Discussion.

Synthesis and Characterization. The synthesis of the platinum(IV) carbamate complexes was accomplished by treating *c,c,t*-[Pt(NH₃)₂Cl₂(OH)₂] with the desired isocyanate in DMF solution (Scheme 2). Because the starting complex, *c,c,t*-[Pt(NH₃)₂Cl₂(OH)₂], is largely insoluble in DMF,

the progress of the reaction was monitored visually by observing conversion of the reaction mixture from a suspension to a homogenous solution. The synthesis of the analogous methyl, ethyl, and isopropyl carbamate complexes has been reported previously.³⁶ In this prior study, the authors prepared these complexes by suspending *c,c,t*-[Pt(NH₃)₂Cl₂(OH)₂] in the neat isocyanate with no additional solvent. In cases where the isocyanate is expensive or toxic, the use of only a slight excess, as demonstrated in the present work, is a clear advantage.

Scheme 2.



The platinum(IV) carbamates are either white (**4 - 6**) or pale yellow to pale orange (**7 - 11**) solids. Compounds **7 - 11** are the first reported platinum(IV) complexes bearing aryl carbamate ligands and thus extend the scope of the chemistry beyond simple alkyl isocyanates. Compounds **4 - 11** exhibit good solubility in DMF and DMSO, moderate solubility in THF, acetoni-

trile, and acetone, and poor solubility in water and halogenated organic solvents. In solution, the aryl carbamate complexes, **7 – 11**, decompose to dark brown solutions when exposed to ambient light over the course of several hours. The alkyl carbamate complexes, **4 – 6**, remain stable in solution even in the presence of light. The aromatic substituents of **7 – 11** most likely play a role in the photodecomposition of the complexes. In the absence of light, all the compounds are stable in solution.

Characterization of compounds **4 – 11** was accomplished by NMR spectroscopy, IR spectroscopy, mass spectrometry, elemental analysis, and X-ray crystallography (*vide infra*). Elemental analyses of the complexes are in good agreement with expected values, and electrospray ionization mass spectrometry gave rise to the expected $[M-H]^-$ signals, further validating the molecular formulas of these compounds. The IR spectra displayed characteristic C=O stretching frequencies ranging from 1647 to 1663 cm^{-1} for the aryl carbamate complexes and 1628 – 1629 cm^{-1} for the alkyl carbamate complexes. All complexes also display N–H stretching frequencies derived from the ammine ligands, which appear as a broad series of bands near 3200 cm^{-1} .

The ^1H , ^{13}C , and ^{19}F (for **10**) NMR spectra of the complexes display all expected resonances. ^{195}Pt and selected ^1H NMR chemical shifts are summarized in Table 3. The signal corresponding to the NH proton of the carbamate ligands is observed between 8.97 – 9.21 ppm for the aryl carbamate complexes, **7 - 11**, and between 6.05 – 6.55 ppm for the alkyl carbamate complexes, **4 - 6**. This 3 ppm shift reflects significant deshielding of the NH carbamate resonance relative to the alkyl substituents by the aryl substituents. The proton resonances of the coordinated ammine ligands appear in all complexes as broad peaks ranging from 6.67 – 6.82 ppm.

These values are consistent with ammine coordination to a Pt(IV) center; protons of amines coordinated to Pt(II) centers typically lie further upfield, between 3 – 5 ppm.⁵⁷

Table 3. ¹⁹⁵Pt and Selected ¹H NMR Shifts for **4** – **11** in DMSO-*d*₆ at 20 °C.

compound	δ ¹⁹⁵ Pt, ppm	δ ¹ H, carbamate	
		NH, ppm	NH ₃ , ppm
4	1276	6.05	6.65
5	1275 (major), 1262(minor)	6.55	6.67
6	1276 (major), 1263 (minor)	6.47	6.67
7	1265	9.12	6.79
8	1264	9.02	6.79
9	1265	8.98	6.77
10	1265	9.21	6.78
11	1269	9.01	6.82

The ¹⁹⁵Pt NMR spectra of **7** – **11** display a single resonance in the range 1264 – 1269 ppm. Given that the known window for ¹⁹⁵Pt NMR shifts is > 15,000 ppm, the small variance in chemical shifts among these complexes indicates that the peripheral substituents of the aryl rings have little effect on the magnetic environment of the platinum nucleus. The alkyl carbamate complex, **4**, exhibits a single ¹⁹⁵Pt NMR resonance in DMSO-*d*₆ at 1276 ppm. These chemical shifts are in the range expected for Pt(IV) complexes^{58, 59} and are close to related platinum(IV) alkyl and aryl carboxylate complexes, which fall between 1000 and 1300 ppm. Although both the ¹H and ¹³C NMR spectra of **5** and **6** are consistent with the presence of a single species in so-

lution, the ^{195}Pt NMR spectra at 20 °C in $\text{DMSO-}d_6$ display two resonances at approximately 1276 and 1262 ppm in relative intensities of approximately 2:1. As the temperature of the NMR sample is increased, the two resonances eventually coalesce (Figure 1 and S1), between 50 and 65 °C. Consistent with the known temperature dependence of ^{195}Pt NMR chemical shifts,⁶⁰ the peaks are shifted downfield at higher temperatures as well.

This fluxional process could also be monitored to by ^1H NMR spectroscopy, as shown in Figures 1 and S1. The NH resonance of the carbamate ligand exhibits a significant temperature dependence, shifting upfield by 0.5 ppm at 80 °C. A small peak in the spectrum near 5.8 ppm broadens into the baseline at 35 °C. This peak most likely corresponds to the NH resonance of a minor conformational isomer. The aliphatic region of the ^1H NMR spectrum is unaffected by changes in temperature. The broad peak of the coordinated NH_3 protons is only slightly affected by an increase in temperature; a small upfield shift occurs and shoulders due to coupling to ^{14}N ($I = 1$) become visible. The changes in the ^{195}Pt and ^1H NMR spectra as a function of temperature are fully reversible; after increasing the temperature to 80 °C, the original spectra can be obtained at 20 °C.

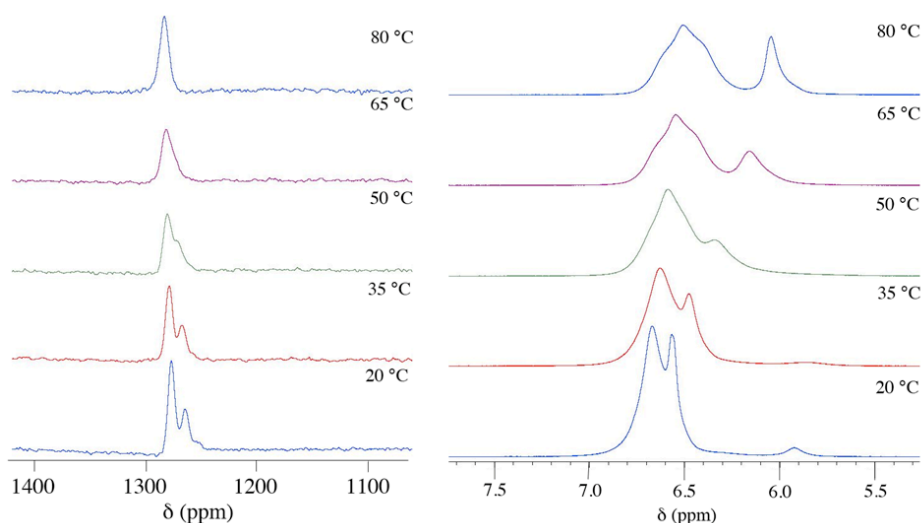
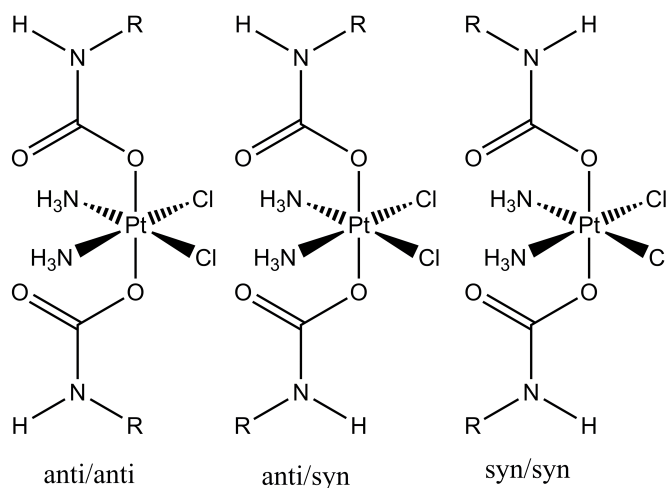


Figure 1. Variable-temperature ^{195}Pt (left) and ^1H (right) NMR spectra of **5** in $\text{DMSO-}d_6$.

As shown in Chart 1, three possible conformational isomers exist for the complexes depending on the orientation of substituents about the C–N bond of the carbamate ligand. It is not clear why only two of these isomers are observed by ^{195}Pt NMR spectroscopy, but it is possible that two of the isomers have very similar chemical shifts and are therefore not resolved as distinct peaks. Another possibility is that one of the conformational isomers is significantly less stable than the other two and never accumulates in a high enough concentration to be observed under equilibrium conditions. The use of variable-temperature ^{195}Pt NMR spectroscopy to distinguish between chemically similar stereoisomers has been reported before.⁶¹⁻⁶⁴ Our findings here similarly validate this method as a valuable tool for distinguishing isomers that could not otherwise be discerned by the more commonly used ^1H and ^{13}C NMR spectroscopy.

Chart 1.



X-ray Crystal Structures. Complexes **4** – **11** were all characterized by X-ray crystallography and are the first such structurally characterized platinum carbamate complexes. Compound **2** was also crystallographically characterized. Information about this structure and the crystal growth

conditions for **2** can be found in the Supporting Information (Figure S2, Tables S1 and S2). Relevant bond distances and angles for the platinum carbamate complexes are listed in Table 4, and the structures are shown in Figures 2 and 3. The bond distances are typical; Pt–Cl bond length are close to 2.3 Å and Pt–O/N distances are ~ 2.0 Å. All complexes display the expected octahedral coordination geometry for platinum(IV). In addition, the structures all have the same stereochemistry as that of the starting platinum(IV) hydroxo compound (*cis,cis,trans*), which is retained upon formation of the carbamate ligands.

Table 4. Selected Interatomic Lengths (Å) and Angles (deg) for **4** – **11**.^a

	4	5	6	7 ^b	8 ^b	9	10 ^b	11
Pt1–Cl1	2.3145(7)	2.3324(6)	2.3075(7)	2.3272(10)	2.3367(9)	2.3187(6)	2.3201(11)	2.3176(6)
Pt1–Cl2	2.3326(8)	2.3170(6)	2.3151(7)	2.3202(10)	2.3324(9)	2.3271(6)	2.3127(11)	2.3126(6)
Pt1–N1	2.037(2)	2.0423(19)	2.042(2)	1.993(3)	2.034(3)	2.029(2)	2.054(4)	2.0299(17)
Pt1–N2	2.037(2)	2.038(2)	2.041(2)	1.995(3)	2.033(3)	2.038(2)	2.048(3)	2.0349(18)
Pt1–O1	2.0117(19)	2.0088(16)	2.026(2)	1.993(3)	2.000(3)	2.0230(18)	2.0209(18)	2.0065(13)
Pt1–O3	2.0062(19)	1.9970(16)	2.001(2)	1.995(3)	2.002(3)	2.0113(18)	1.9936(19)	2.0161(13)
N1–Pt1–N2	90.00(10)	90.02(8)	93.17(10)	92.21(13)	89.81(14)	91.70(9)	93.49(10)	92.42(7)
Cl1–Pt1–Cl2	92.57(3)	91.99(2)	91.48(3)	92.68(4)	94.64(3)	90.90(2)	89.24(3)	91.33(2)
O1–Pt1–N1	96.54(9)	86.31(7)	97.67(10)	96.66(12)	91.99(13)	91.27(8)	91.90(14)	91.81(6)
O1–Pt1–Cl2	90.12(6)	87.53(5)	90.47(6)	86.18(8)	88.04(9)	88.69(6)	89.58(10)	88.74(4)
O3–Pt1–N2	94.89(9)	89.31(8)	93.21(9)	93.15(12)	92.70(13)	91.94(8)	91.40(14)	96.96(6)
O3–Pt1–Cl1	87.04(6)	88.30(5)	89.64(6)	88.14(8)	87.07(9)	87.92(5)	87.67(9)	84.12(4)
O1–Pt1–O3	174.06(8)	174.22(7)	174.17(9)	174.94(11)	168.70(11)	174.20(7)	174.72(8)	173.33(6)

^aThe numbers in parentheses are the estimated standard deviations of the last significant figures. Atoms are labeled as indicated in Figures 2 and 3.

^bTwo molecules per asymmetric unit are present in the crystal lattice. The parameters shown here are only for one of those molecules.

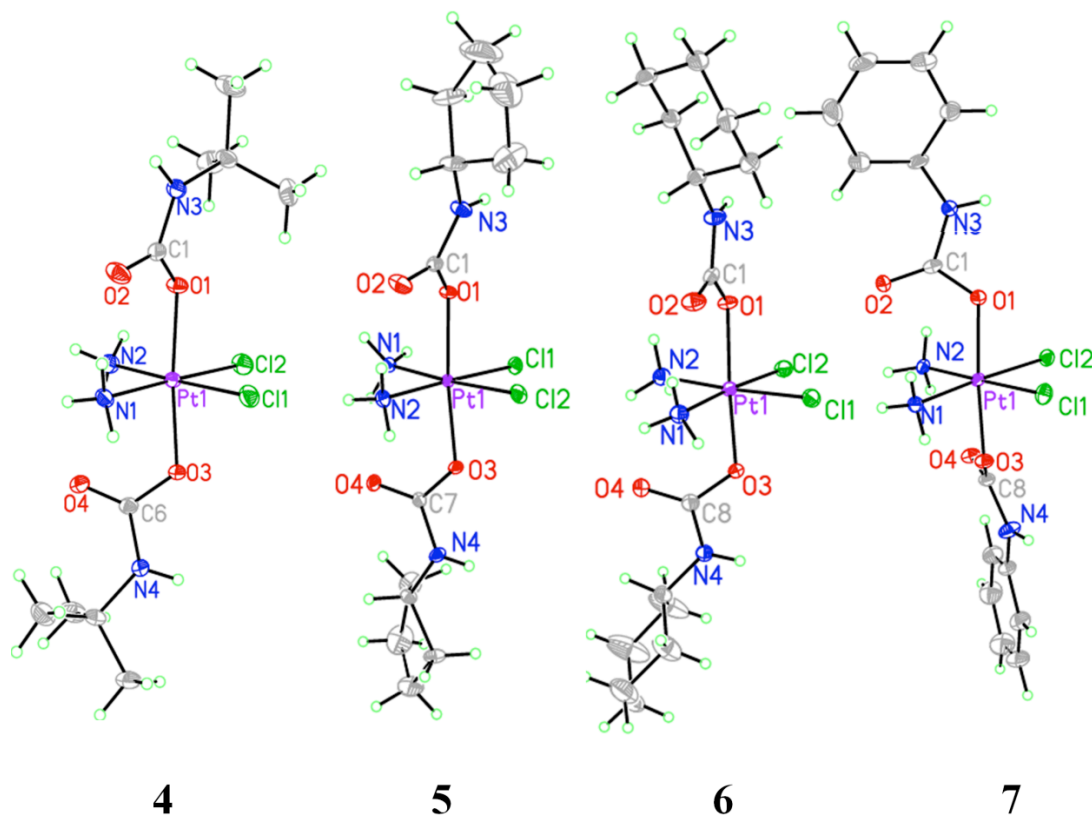


Figure 2. Molecular structures of **4** – **7**. Ellipsoids are drawn at the 50% probability level.

A common feature among the eight complexes is the presence of intramolecular hydrogen bonding between the oxygen atom of the axial carbamate ligands and the equatorial ammine ligands. Three different geometries are observed for this interaction, as shown in Figure 4. In the first geometry, the oxygen atoms lie in a plane bisecting the N–Pt–N angle and interact with both coordinated amines equally. This situation occurs for **6**, both molecules in the asymmetric unit of **7**, one of the molecules in the asymmetric unit of **8**, and **11**. The geometry in which both of the oxygen atoms are twisted to opposite sides and hydrogen bond with the different amines is observed only in the case of **5**. In the final case, one of the oxygen atoms is twisted off to the side and interacts with only one of the coordinated amines. This geometry is the most common hydrogen bonding motif for this class of compounds and occurs in the remaining structures.

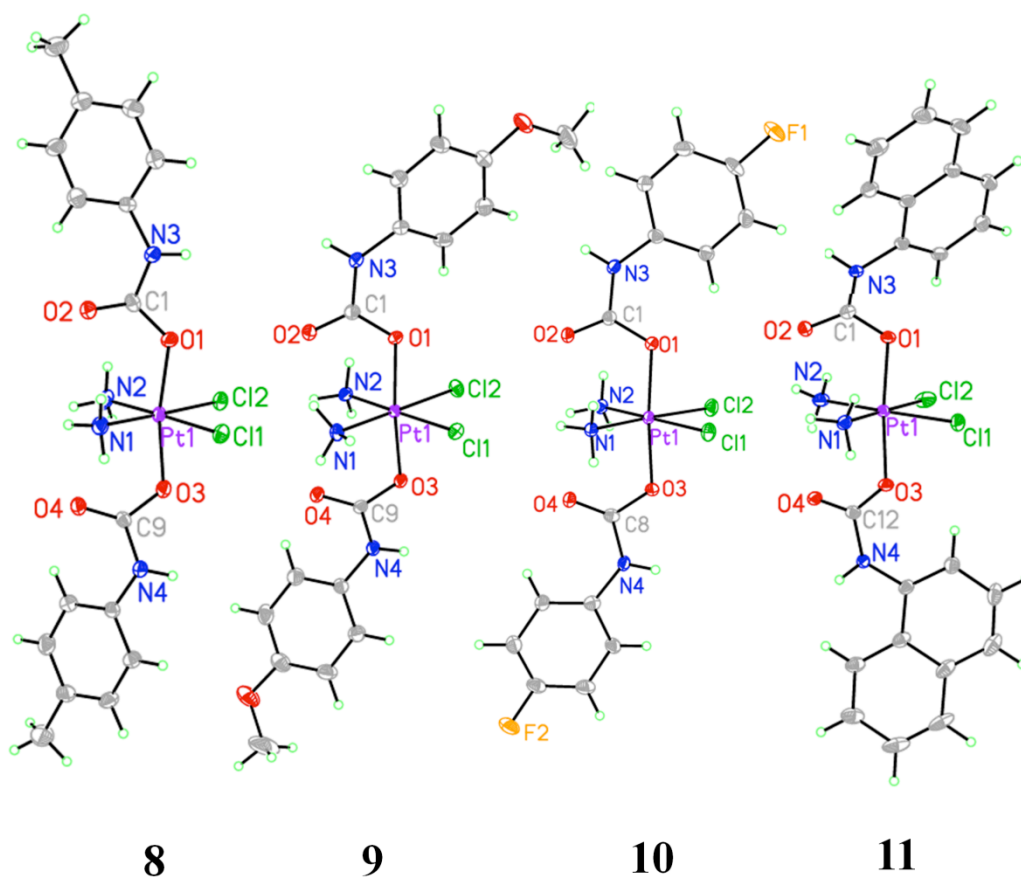


Figure 3. Molecular structures of **8** – **11**. Ellipsoids are drawn at the 50% probability level.

As discussed above, different conformational isomers, reflecting alternative orientations of substituents about the carbamate C–N bond, exist (Chart 1). The most commonly observed isomer is that with a *syn/syn* ligand orientation, observed for **5**, **6**, both molecules in the asymmetric unit of **7**, both molecules in the asymmetric unit of **8**, and one of the molecules in the asymmetric unit of **10**. The *anti/syn* isomer occurs in **4**, **9**, and the other molecule in the asymmetric unit of **10**. The naphthyl carbamate complex **11** crystallized exclusively as the *anti/anti* isomer. The occurrence of all three possible isomers throughout the crystal structures of **4** – **11** reflects a small energy difference between isomers in solution, as observed by NMR spectroscopy.

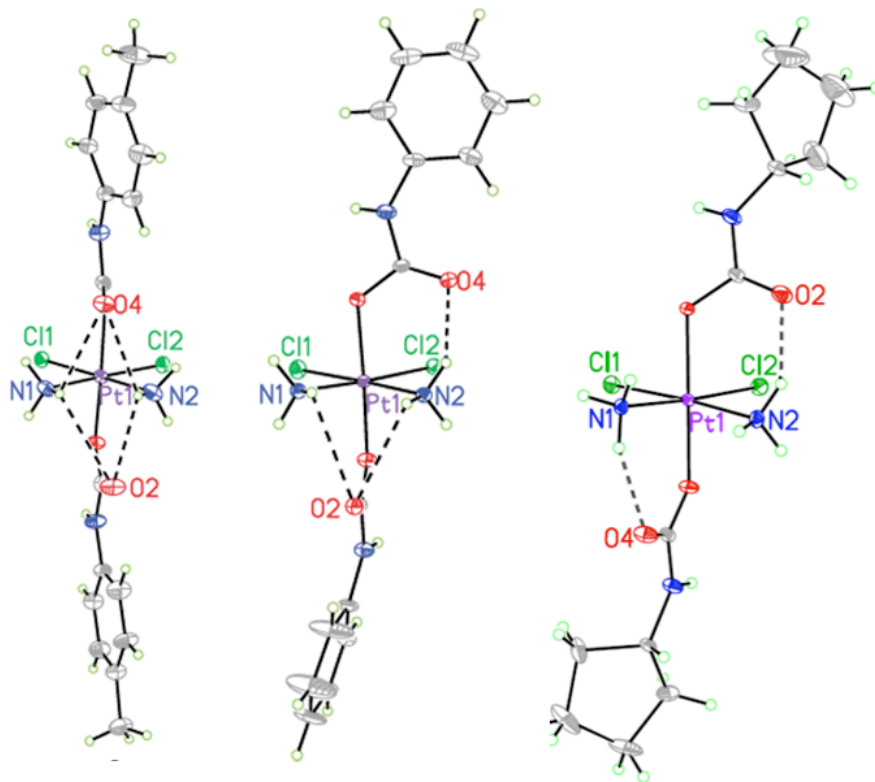


Figure 4. The three intramolecular hydrogen bonding motifs observed in the crystal structures of **4 – 11**. These three examples are compounds **8** (left), **7** (middle), and **5** (right).

Cyclic Voltammetry. The biological activity of platinum(IV) complexes is mediated by their redox chemistry. In most cases, platinum(IV) complexes, unlike their platinum(II) progeny, do not bind directly to DNA or other biological nucleophiles.⁶⁵ The redox potential of platinum(IV) complexes is therefore believed to be an important factor in their efficacy as antitumor agents. With this possibility in mind, we studied redox potentials of **1 – 11** by cyclic voltammetry.

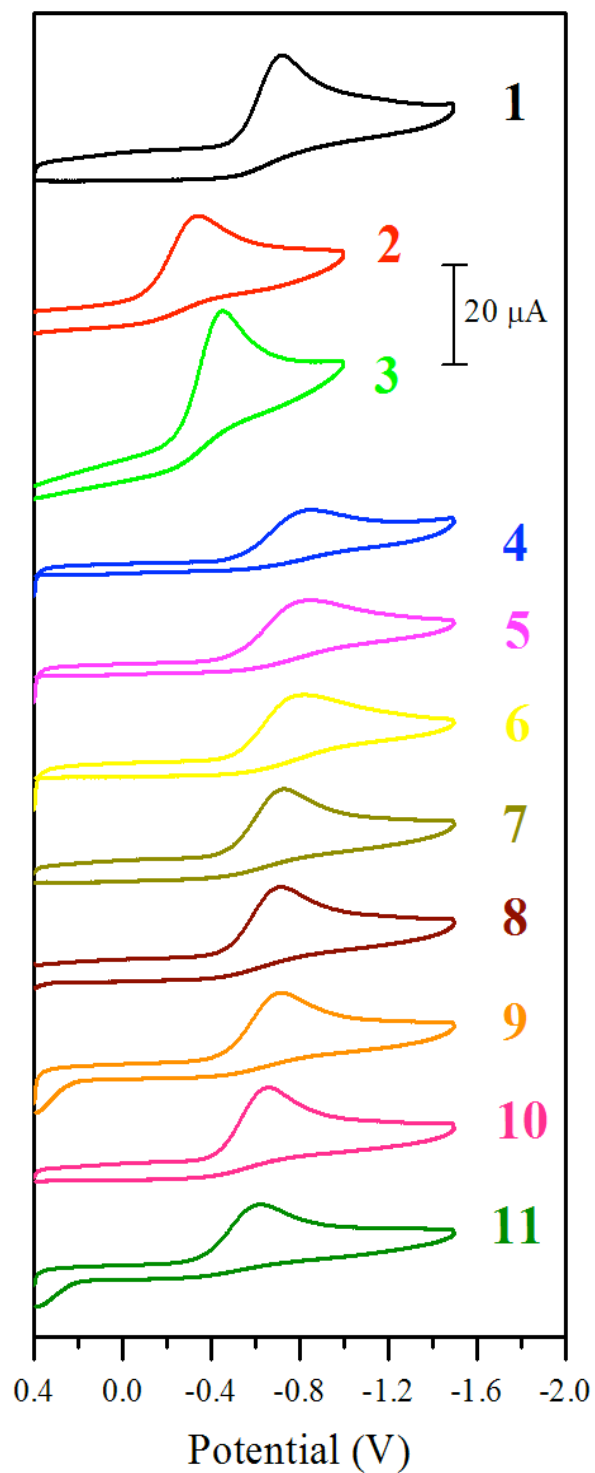


Figure 5. Cyclic voltammograms of **1** – **11**. Data obtained for 2 mM solutions of the complexes in DMF with 0.1 M (*n*-Bu₄N)PF₆ as the supporting electrolyte. The scan rate was 100 mV/s.

Because of the limited aqueous solubility of **4** – **11**, the cyclic voltammograms were recorded in DMF using 0.1 M (*n*-Bu₄N)PF₆ as the supporting electrolyte. For comparison, the electrochemical properties of the compounds *c,c,t*-[Pt(NH₃)₂Cl₂(O₂CCH₃)₂] (**1**), *c,c,t*-[Pt(NH₃)₂Cl₂(O₂CCF₃)₂] (**2**), and *cis*-[Pt(NH₃)₂Cl₄] (**3**) were also investigated by cyclic voltammetry in the same solvent and electrolyte system. As expected for the Pt(IV)/Pt(II) redox couple, all of the compounds exhibit a single irreversible reduction event in the potential window of +0.4 to -1.2 V vs. Ag/AgCl. The peak potentials (E_p) for these processes obtained at a scan rate of 100 mV/s are reported in Table 5 and the corresponding cyclic voltammograms are shown in Figure 5.

Table 5. Peak Reduction Potentials for **1** – **11** Measured by Cyclic Voltammetry in DMF.

Compound	E_p , V vs. Ag/AgCl
1	-0.72 (-0.64) ^{a,b}
2	-0.35 (0.01) ^{a,c}
3	-0.45 (-0.26) ^{a,b}
4	-0.85
5	-0.85
6	-0.82
7	-0.73
8	-0.71
9	-0.72
10	-0.66
11	-0.63

^aValues in parentheses are for those measured in aqueous solution. ^bRef. 66. ^cThis work (Figure S3, SI).

For a given set of equatorial ligands on a platinum(IV) center, the reduction potential in water predictably changes as the axial ligands are varied.^{18,66} Trifluoroacetate ligands produce the most easily reduced (highest redox potential) platinum(IV) complexes, followed by chloride ligands, and then acetate ligands in that order. Axial hydroxo ligands, although not investigated here, give rise to platinum(IV) complexes that are even more difficult to reduce than those with acetate ligands. For example, the precursor complex *c,c,t*-[Pt(NH₃)₂Cl₂(OH)₂] is reported to have a very negative peak potential at -880 mV in aqueous media.⁶⁶ In moving from water to DMF, we find here that this general trend still exists for the chloride and carboxylate ligands, as $E_p(\mathbf{2}) > E_p(\mathbf{3}) > E_p(\mathbf{1})$. The peak potentials themselves, however, are shifted significantly from those measured in water. In water, the measured peak potentials of **1** and **3** have been determined by others to be -635 and -260 mV, respectively,⁶⁶ and the peak potential of **8** was measured to be 5 mV (Figure S3). In DMF, these potentials are -722 (**1**), -345 (**2**), and -454 (**3**) mV, indicating that this solvent change decreases the reduction potential by up to 300 mV. Even though the potentials measured in DMF are shifted significantly from those measured in aqueous solution, a comparison of peak potentials for the carbamate complexes **4** – **11** to those for **1** – **3** is valuable for understanding the relative stability of the complexes in the biological milieu.

Compounds **7** – **9** display nearly identical peak potentials near -720 mV. This similarity indicates that electron-donating groups in the para position of the aryl carbamate ligands have little effect on the redox potentials of these compounds. Notably, the peak potentials of these compounds are indistinguishable from that of **1**. Thus the aryl carbamate ligands confer the same degree of stabilization to the +4 oxidation state as the acetate ligand. Compound **10** exhibits a higher peak potential at -655 mV. This higher potential is attributed to the electron-withdrawing fluorine atom on the aromatic ring of the carbamate ligand, which favors reduction. The least

negative peak potential of the series, at -625 mV, is displayed by the naphthyl carbamate complex **11**. The reason for **11** having a peak potential ≥ 100 mV more positive than those of **7** – **9** is not entirely clear. A possible explanation is that the increased steric bulk from the large naphthyl group favors ligand dissociation and consequently reduction. The alkyl carbamates **4** – **6** have peak potentials between -820 and -850 mV. The alkyl substituents on the carbamate ligand stabilize the +4 oxidation state by about 100 mV relative to the aryl substituents. This observation indicates that the alkyl carbamates are stronger electron donors and are more capable of stabilizing the electron-poor +4 oxidation state than the aryl carbamates.

Theoretical Calculations. Geometry optimizations were carried out for **1** – **11** at the DFT B3LYP theoretical level. For the carbamate complexes, **4** – **11**, geometry optimizations were computed only for the anti/anti isomers (Chart 1). Although no symmetry restraints were placed on the geometry optimizations, all optimized structures attained nearly perfect C_{2v} symmetry with the principal 2-fold axis bisecting the Cl–Pt–Cl and NH_3 –Pt– NH_3 angles in the equatorial plane. In this configuration, intramolecular hydrogen bonding occurs between the oxygen atom of the carbamate ligands and both of the coordinated ammine ligand, as observed experimentally in several of the crystal structures.

The frontier molecular orbits (FMOs) of **1** – **3** are shown in a qualitative molecular orbital diagram in Figure 6. The expected two-over-three d-orbital splitting for a nearly octahedral transition metal complex is predicted by these computations. The LUMO and LUMO+1 are nearly degenerate and are d_{z^2} and d_{xy} σ^* in character. The HOMO to HOMO-3 molecular orbitals are also close in energy. These orbitals are $d_{x^2-y^2}$, d_{xz} , and d_{yz} π^* , and Cl 3p non-bonding in character. The HOMO-LUMO gaps of **1**, **2**, and **3** are 4.16, 3.97, and 3.70 eV respectively. These

values correspond to the magnitude of the d-orbital splitting and reflect the ordering of the acetate, trifluoroacetate, and chloride ligands in the spectrochemical series.

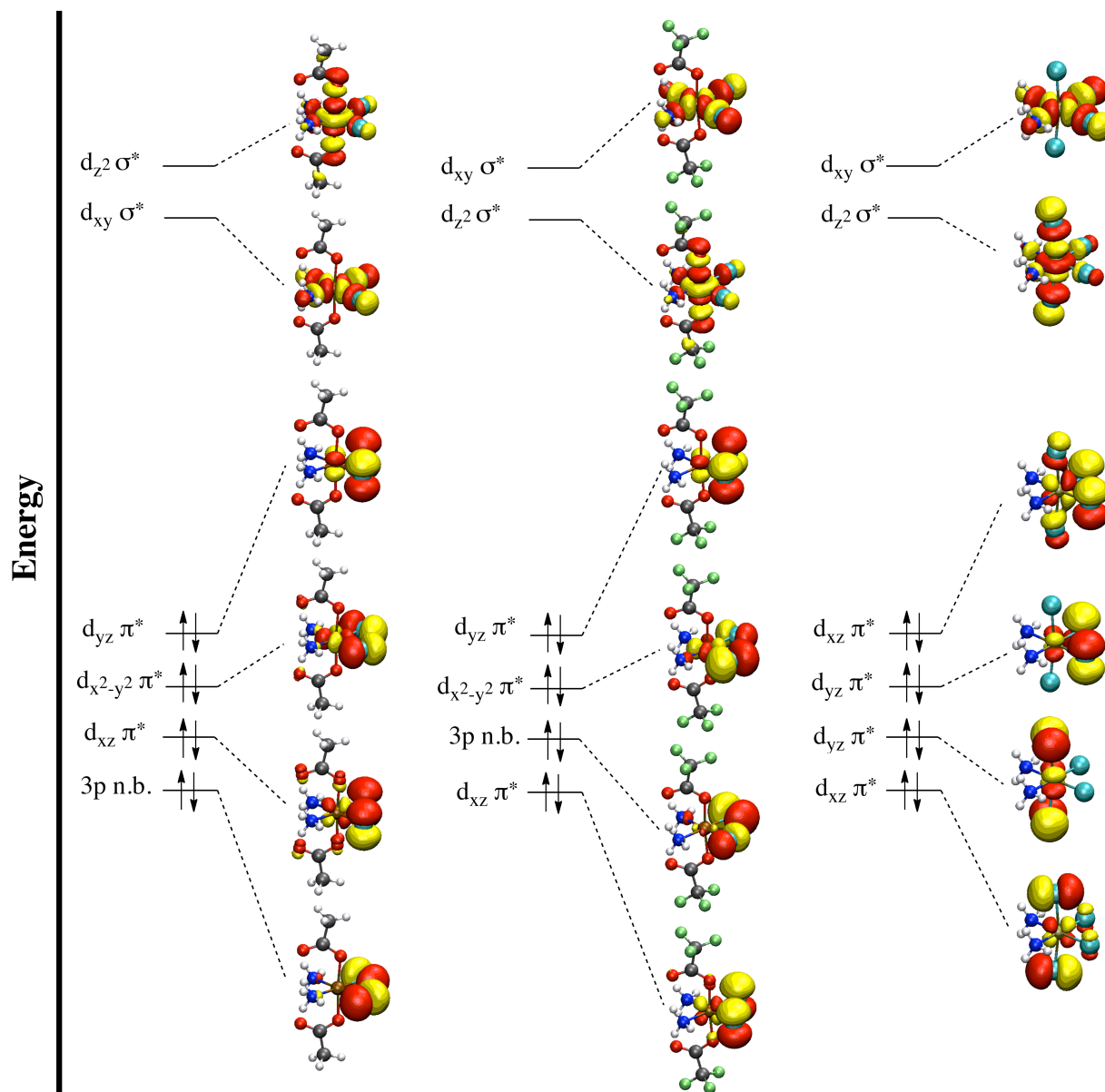


Figure 6. Qualitative molecular orbital diagrams for **1** (left), **2** (middle), and **3** (right).

The FMOs of **6**, **7**, and **11** are shown in the qualitative molecular orbital diagram in Figure 7. The FMOs of the other alkyl carbamate complexes, **4** and **5**, are qualitatively similar to

those of **6**, as are the FMOs of the other aryl carbamate complexes, **8** – **10**, to complex **7**. Like **1** – **3**, the LUMO and LUMO+1 of the carbamate complexes are d_{z^2} and $d_{xy} \sigma^*$ in character. The HOMOs, however, are ligand-localized π orbitals. The presence of these orbitals leads to smaller HOMO-LUMO gaps for the aryl carbamate complexes, which range from 2.52 – 2.99 eV, compared to those of **1** – **3**. This result is consistent with the observation that **7** – **11** are sensitive to light. The smaller HOMO-LUMO gap may render dissociative excited states accessible by the energy provided by visible light.

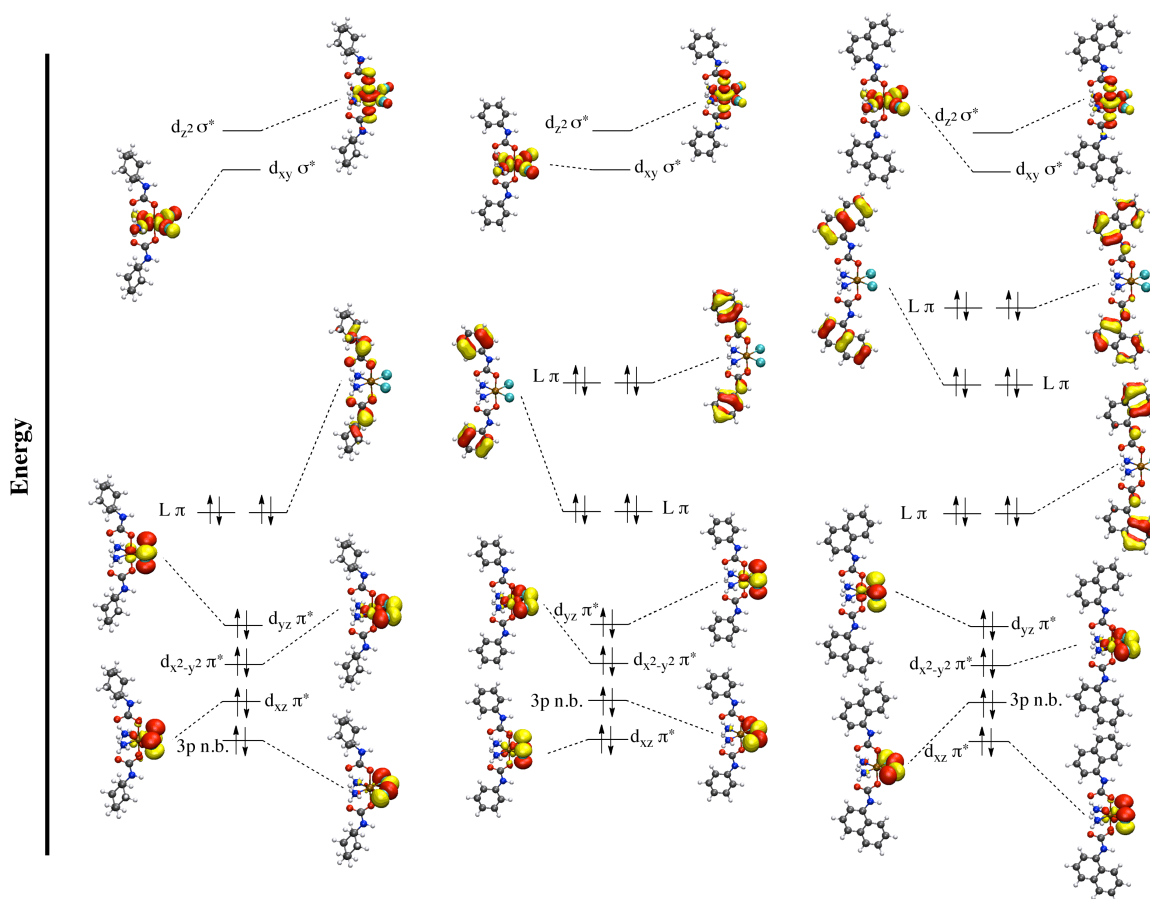


Figure 7. Qualitative molecular orbital diagram for **6** (left), **7** (middle), and **11** (right).

The gas-phase adiabatic electron affinities of **1**, **2**, and **4** – **11** were computed by optimizing the geometry of the 1-electron reduced Pt(III) species as a doublet anion, and then subtracting its total energy from the neutral Pt(IV) species. The results are summarized

subtracting its total energy from the neutral Pt(IV) species. The results are summarized in Table 6. The optimized geometries of the Pt(III) species give rise to stationary points on

Table 6. Computed Adiabatic Electron Affinities and the Difference in Computed Interatomic Distances between the Neutral Pt(IV) Complex and the Anionic Pt(III) Complex.^a

Compound	Electron Affinity, eV	$\Delta d, \text{\AA}$					
		Pt–Cl1	Pt–Cl2	Pt–N1	Pt–N2	Pt–O1	Pt–O2
1	2.754	0.03021	0.03005	-0.01439	-0.01425	0.39707	0.39701
2	3.791	0.02479	0.02553	-0.02139	-0.02078	0.40872	0.41175
4	2.576	0.02695	0.02698	-0.00836	-0.00832	0.39533	0.39631
5	2.570	0.02719	0.02718	-0.00791	-0.00790	0.39420	0.39422
6	2.321	0.36070	0.03682	-0.01119	0.33653	0.02840	0.02918
7	2.683	0.33739	0.03196	-0.01319	0.33328	0.03518	0.03507
8	2.631	0.33878	0.03234	-0.01287	0.33366	0.03467	0.03458
9	2.901	0.02454	0.02454	-0.00784	-0.00787	0.39023	0.39024
10	3.129	0.02412	0.02419	-0.00897	-0.00884	0.39158	0.39165
11	3.060	0.02305	0.02306	-0.00790	-0.00792	0.39017	0.39028

^aAtoms are labeled as shown in Figures 2 and 3.

the potential energy surface, as evidenced by the lack of imaginary frequencies except in the case of **3**. A comparison of geometrical parameters of the calculated Pt(IV) and Pt(III) structures is presented in Table 6. Upon reduction to Pt(III), two mutually trans bond are elongated significantly whereas the other bonds are only altered slightly. This result is expected, for the addition of another electron to the closed-shell Pt(IV) species would require population of an antibonding orbital. For most cases, the axial platinum-carbamate bond is lengthened by approximately 0.4 Å in the Pt(III) complex, which is consistent with the conventional view of Pt(IV) reduction de-

pictured in Scheme 1. For **6** – **8**, however, significant bond elongation occurs for the equatorial, mutually trans platinum-chloride and platinum-ammine bonds. These bonds are elongated by approximately 0.34 Å. This result suggests that in some cases elimination of the equatorial ligands may be a viable reductive pathway of platinum(IV) and is consistent with experimental observation of this pathway by others.⁶⁷⁻⁶⁹ The computed gas phase adiabatic electron affinities correlate well with the observed peak potentials for reduction. In Figure 8, the peak potentials are plotted as a function of the electron affinity. The relationship is roughly linear ($R^2 = 0.887$) and, as expected, larger electron affinities correlate with more positive peak potentials.

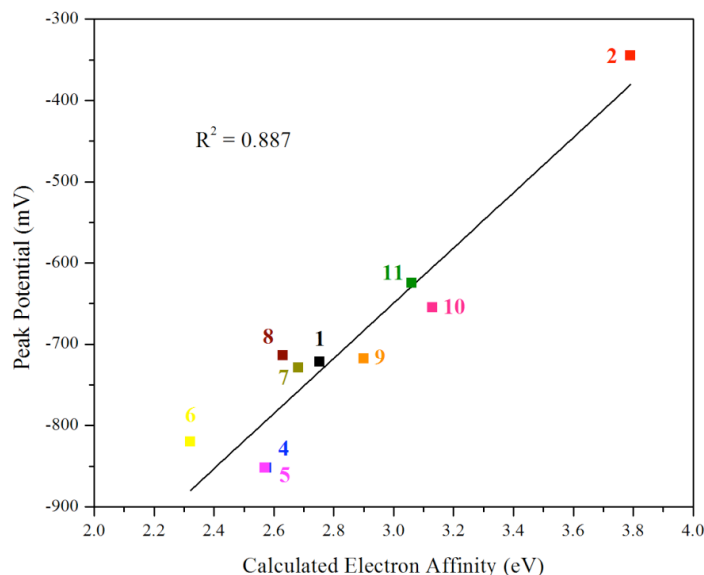


Figure 8. Plot of the computed adiabatic electron affinity versus the experimentally measured reduction peak potentials. The black line is the least squares best fit through of the data.

Biological Properties. The cytotoxicities of compounds **4** – **11** and cisplatin against human lung carcinoma (A549) and human normal lung (MRC-5) cells were measured by the MTT assay. The results are shown in Table 7, and dose-response curves can be found in Figures S4 and S5. In A549 cells, most of the platinum(IV) carbamates exhibit a level of cytotoxicity that is similar to that of cisplatin. The IC_{50} values range from 3 to 6.7 μ M, compared to an IC_{50} of 7.0 μ M for cis-

platin. Compounds **4** and **5**, bearing tert-butyl and cyclopentyl carbamate ligands, showed greater cytotoxicity than the other compounds, the IC_{50} values being 1.0 and 0.6 μM , respectively. In the non-cancerous lung fibroblasts (MRC-5), all the complexes, except for **4** and **5**, were slightly less cytotoxic than cisplatin. The IC_{50} of cisplatin in this cell line was 4.3 μM and those of **6** – **11** ranged from 4.8 to 16.0 μM . The cytotoxicities of **4** and **5** in the lung fibroblasts were marked by IC_{50} values of 2.8 and 2.3 μM , indicating that they are approximately a factor of 2 less cytotoxic in the healthy cells compared to the cancerous cells, as observed for the other carbamate complexes. The results here demonstrate that, like the platinum(IV) complexes bearing axial chloro, hydroxo, and acetato ligands, this newly synthesized class of platinum(IV) complexes bearing axial carbamate ligands are also viable anticancer drug candidates.

Table 7. Cytotoxicities of Cisplatin and **4** – **11** in A549 and MRC-5 Cells.

compound	IC_{50} (μM) ^a	
	A549	MRC-5
4	1.0 ± 0.3	2.8 ± 0.8
5	0.6 ± 0.3	2.3 ± 0.7
6	6.7 ± 2.9	12.7 ± 3.5
7	6.7 ± 2.1	16.0 ± 6.6
8	3.0 ± 1.0	5.1 ± 1.8
9	5.3 ± 2.5	9.3 ± 3.2
10	3.7 ± 1.2	7.6 ± 3.1
11	4.3 ± 1.5	4.8 ± 0.3
cisplatin	7.0 ± 2.6	4.3 ± 1.3

^a IC_{50} values, the concentrations of platinum where cell growth is inhibited by 50% compared to controls run in the absence of added complexes, measured by the MTT assay following a 72-h exposure. Values are the average of at least three independent experiments, and the reported errors are the corresponding standard deviations.

Conclusions

The synthesis of eight new platinum(IV) carbamate complexes is described. The general reactivity of both aryl and alkyl isocyanates with the important platinum(IV) synthon, *c,c,t*-[Pt(NH₃)₂Cl₂(OH)₂], provides a valuable synthetic methodology for the design of new platinum(IV) complexes with novel properties. It also offers a route for the functionalization of isocyanate-bearing nanomaterials through the formation of a platinum carbamate bond. In contrast to the more common platinum(IV) carboxylate complexes, platinum(IV) carbamates adopt different isomeric forms depending on the rotational orientation of the ligand, as revealed by NMR spectroscopy and X-ray crystallography, and their ligand-based orbitals are intermediate in energy between those of the empty and filled metal d-orbitals, as determined by DFT calculations. Electrochemical studies of the platinum(IV) carbamates reveal redox potentials similar to those of the platinum(IV) acetates, such as satraplatin. This result suggests that platinum(IV) carbamate complexes should exhibit similar stability properties in biological milieu as the acetate complexes. The fact that the platinum(IV) carbamates display cytotoxicities similar to or better than cisplatin reveals their therapeutic potential. Finally, DFT computational analyses indicate that the redox potential of platinum(IV) complexes can be correlated with their computed electron affinities, corroborating experimentally deduced reduction pathways.

Acknowledgement. This work was supported by Grant CA034992 from the National Cancer Institute. Spectroscopic instrumentation at the MIT DCIF is maintained with funding from NIH Grant 1S10RR13886-01.

Supporting Information Available: X-ray crystallographic data in CIF format, crystal growth and refinement details, crystallographic data collection and refinement parameters for **2** (Table S1), selected interatomic distances and angles for **2** (Table S2), XYZ coordinates, energies, and lowest frequencies for all geometry optimized compounds (Tables S3 – S23), VT-NMR spectra of **6** (Figure S1), ORTEP diagram of **2** (Figure S2), cyclic voltammogram of **2** in water (Figure S3), and dose-response curves for A549 (Figure S4) and MRC-5 cells (Figure S5). This material is available free of charge via the Internet at <http://pubs.acs.org>.

References

- (1) Kelland, L. *Nat. Rev. Cancer* **2007**, *7*, 573-584.
- (2) Bancroft, D. P.; Lepre, C. A.; Lippard, S. J. *J. Am. Chem. Soc.* **1990**, *112*, 6860-6871.
- (3) Davies, M. S.; Berners-Price, S. J.; Hambley, T. W. *Inorg. Chem.* **2000**, *39*, 5603-5613.
- (4) Takahara, P. M.; Rosenzweig, A. C.; Frederick, C. A.; Lippard, S. J. *Nature* **1995**, *377*, 649-652.
- (5) Spingler, B.; Whittington, D. A.; Lippard, S. J. *Inorg. Chem.* **2001**, *40*, 5596-5602.
- (6) Silverman, A. P.; Bu, W.; Cohen, S. M.; Lippard, S. J. *J. Biol. Chem.* **2002**, *277*, 49743-49749.
- (7) Todd, R. C.; Lippard, S. J. *J. Inorg. Biochem.* **2010**, *104*, 902-908.
- (8) Jung, Y.; Lippard, S. J. *Chem. Rev.* **2007**, *107*, 1387-1407.
- (9) Todd, R. C.; Lippard, S. J. *Metallomics* **2009**, *1*, 280-291.
- (10) Daugaard, G.; Abildgaard, U. *Cancer Chemother. Pharmacol.* **1989**, *25*, 1-9.
- (11) Cvitkovic, E. *Cancer Treat. Rev.* **1998**, *24*, 265-281.
- (12) Screnci, D.; McKeage, M. J. *J. Inorg. Biochem.* **1999**, *77*, 105-110.
- (13) Hall, M. D.; Hambley, T. W. *Coord. Chem. Rev.* **2002**, *232*, 49-67.
- (14) Hall, M. D.; Dolman, R. C.; Hambley, T. W. *Met. Ions Biol. Syst.* **2004**, *42*, 297-322.
- (15) Hall, M. D.; Mellor, H. R.; Callaghan, R.; Hambley, T. W. *J. Med. Chem.* **2007**, *50*, 3403-3411.
- (16) Wheate, N. J.; Walker, S.; Craig, G. E.; Oun, R. *Dalton Trans.* **2010**, *39*, 8113-8127.
- (17) Ellis, L. T.; Er, H. M.; Hambley, T. W. *Aust. J. Chem.* **1995**, *48*, 793-806.
- (18) Choi, S.; Filotto, C.; Bisanzo, M.; Delaney, S.; Lagasee, D.; Whitworth, J. L.; Jusko, A.; Li, C.; Wood, N. A.; Willingham, J.; Schwenker, A.; Spaulding, K. *Inorg. Chem.* **1998**, *37*, 2500-2504.
- (19) Battle, A. R.; Deacon, G. B.; Dolman, R. C.; Hambley, T. W. *Aust. J. Chem.* **2002**, *55*, 699-704.

- (20) Platts, J. A.; Hibbs, D. E.; Hambley, T. W.; Hall, M. D. *J. Med. Chem.* **2001**, *44*, 472-474.
- (21) Gramatica, P.; Papa, E.; Luini, M.; Monti, E.; Gariboldi, M. B.; Ravera, M.; Gabano, E.; Gaviglio, L.; Osella, D. *J. Biol. Inorg. Chem.* **2010**, *15*, 1157-1169.
- (22) Reithofer, M. R.; Bytzek, A. K.; Valiahdi, S. M.; Kowol, C. R.; Groessler, M.; Hartinger, C. G.; Jakupec, M. A.; Galanski, M.; Keppler, B. K. *J. Inorg. Biochem.* **2011**, *105*, 46-51.
- (23) Barnes, K. R.; Kutikov, A.; Lippard, S. J. *Chem. Biol.* **2004**, *11*, 557-564.
- (24) Mukhopadhyay, S.; Barnés, C. M.; Haskel, A.; Short, S. M.; Barnes, K. R.; Lippard, S. J. *Bioconjugate Chem.* **2008**, *19*, 39-49.
- (25) Dhar, S.; Lippard, S. J. *Proc. Natl. Acad. Sci. U. S. A.* **2009**, *106*, 22199-22204.
- (26) Ang, W. H.; Khalaila, I.; Allardyce, C. S.; Juillerat-Jeanneret, L.; Dyson, P. J. *J. Am. Chem. Soc.* **2005**, *127*, 1382-1383.
- (27) Reithofer, M. R.; Valiahdi, S. M.; Galanski, M.; Jakupec, M. A.; Arion, V. B.; Keppler, B. K. *Chem. Biodivers.* **2008**, *5*, 2160-2170.
- (28) Feazell, R. P.; Nakayama-Ratchford, N.; Dai, H.; Lippard, S. J. *J. Am. Chem. Soc.* **2007**, *129*, 8438-8439.
- (29) Dhar, S.; Liu, Z.; Thomale, J.; Dai, H. J.; Lippard, S. J. *J. Am. Chem. Soc.* **2008**, *130*, 11467-11476.
- (30) Rieter, W. J.; Pott, K. M.; Taylor, K. M. L.; Lin, W. J. *J. Am. Chem. Soc.* **2008**, *130*, 11584-11585.
- (31) Dhar, S.; Daniel, W. L.; Giljohann, D. A.; Mirkin, C. A.; Lippard, S. J. *J. Am. Chem. Soc.* **2009**, *131*, 14652-14653.
- (32) Taylor-Pashow, K. M. L.; Rocca, J. D.; Xie, Z.; Tran, S.; Lin, W. J. *J. Am. Chem. Soc.* **2009**, *131*, 14261-14263.
- (33) Aryal, S.; Hu, C.-M. J.; Zhang, L. *ACS Nano* **2010**, *4*, 251-258.
- (34) Duong, H. T. T.; Huynh, V. T.; de Souza, P.; Stenzel, M. H. *Biomacromolecules* **2010**, *11*, 2290-2299.
- (35) Min, Y.; Mao, C.; Xu, D.; Wang, J.; Liu, Y. *Chem. Commun.* **2010**, *46*, 8424-8426.
- (36) Giandomenico, C. M.; Abrams, M. J.; Murrer, B. A.; Vollano, J. F.; Rheinheimer, M. I.; Wyer, S. B.; Bossard, G. E.; Higgins, J. D., III *Inorg. Chem.* **1995**, *34*, 1015-1021.
- (37) Barnard, C. F. J.; Vollano, J. F.; Chaloner, P. A.; Dewa, S. Z. *Inorg. Chem.* **1996**, *35*, 3280-3284.
- (38) Galanski, M.; Keppler, B. K. *Inorg. Chem.* **1996**, *35*, 1709-1711.
- (39) Galanski, M.; Keppler, B. K. *Inorg. Chim. Acta* **1997**, *265*, 271-274.
- (40) Ang, W. H.; Pilet, S.; Scopelliti, R.; Bussy, F.; Juillerat-Jeanneret, L.; Dyson, P. J. *J. Med. Chem.* **2005**, *48*, 8060-8069.
- (41) Reithofer, M.; Galanski, M.; Roller, A.; Keppler, B. K. *Eur. J. Inorg. Chem.* **2006**, 2612-2617.
- (42) Reithofer, M. R.; Valiahdi, S. M.; Jakupec, M. A.; Arion, V. B.; Egger, A.; Galanski, M.; Keppler, B. K. *J. Med. Chem.* **2007**, *50*, 6692-6699.
- (43) Kelland, L. R.; Barnard, C. F. J.; Evans, I. G.; Murrer, B. A.; Theobald, B. R. C.; Wyer, S. B.; Goddard, P. M.; Jones, M.; Valenti, M.; Bryant, A.; Rogers, P. M.; Harrap, K. R. *J. Med. Chem.* **1995**, *38*, 3016-3024.
- (44) Hall, M. D.; Dillon, C. T.; Zhang, M.; Beale, P.; Cai, Z. H.; Lai, B.; Stampfl, A. P. J.; Hambley, T. W. *J. Biol. Inorg. Chem.* **2003**, *8*, 726-732.

- (45) Davies, M. S.; Hall, M. D.; Berners-Price, S. J.; Hambley, T. W. *Inorg. Chem.* **2008**, *47*, 7673-7680.
- (46) *APEX2*, 2008-4.0; Bruker AXS, Inc.: Madison, WI, 2008.
- (47) Sheldrick, G. M. *SADABS: Area-Detector Absorption Correction*, University of Göttingen: Göttingen, Germany, 2008.
- (48) Sheldrick, G. M. *SHELXTL-97*, 6.14; University of Göttingen: Göttingen, Germany, 2000.
- (49) Sheldrick, G. M. *Acta Crystallogr. Sect. A* **2008**, *64*, 112-122.
- (50) Spek, A. L. *PLATON, A Multipurpose Crystallographic Tool*, Utrecht University: Utrecht, The Netherlands, 2008.
- (51) Müller, P. *Crystallogr. Rev.* **2009**, *15*, 57-83.
- (52) Frisch, M. J.; Trucks, G. W.; Schlegel, H. B.; Scuseria, G. E.; Robb, M. A.; Cheeseman, J. R.; J. A. Montgomery, J.; Vreven, T.; Kudin, K. N.; Burant, J. C.; Millam, J. M.; Iyengar, S. S.; Tomasi, J.; Barone, V.; Mennucci, B.; Cossi, M.; Scalmani, G.; Rega, N.; Petersson, G. A.; Nakatsuji, H.; Hada, M.; Ehara, M.; Toyota, K.; Fukuda, R.; Hasegawa, J.; Ishida, M.; Nakajima, T.; Honda, Y.; Kitao, O.; Nakai, H.; Klene, M.; Li, X.; Knox, J. E.; Hratchian, H. P.; Cross, J. B.; Bakken, V.; Adamo, C.; Jaramillo, J.; Gomperts, R.; Stratmann, R. E.; Yazyev, O.; Austin, A. J.; Cammi, R.; Pomelli, C.; Ochterski, J. W.; Ayala, P. Y.; Morokuma, K.; Voth, G. A.; Salvador, P.; Dannenberg, J. J.; V. G. Zakrzewski; Dapprich, S.; Daniels, A. D.; Strain, M. C.; Farkas, O.; Malick, D. K.; Rabuck, A. D.; Raghavachari, K.; Foresman, J. B.; Ortiz, J. V.; Cui, Q.; Baboul, A. G.; Clifford, S.; Cioslowski, J.; Stefanov, B. B.; Liu, G.; Liashenko, A.; Piskorz, P.; Komaromi, I.; Martin, R. L.; Fox, D. J.; Keith, T.; Al-Laham, M. A.; Peng, C. Y.; Nanayakkara, A.; Challacombe, M.; Gill, P. M. W.; Johnson, B.; Chen, W.; Wong, M. W.; Gonzalez, C.; Pople, J. A. *Gaussian 03*, Revision D.01; Gaussian, Inc.: Wallingford, CT, 2004.
- (53) Lee, C.; Yang, W.; Parr, R. G. *Phys. Rev. B* **1988**, *37*, 785-789.
- (54) Becke, A. D. *J. Chem. Phys.* **1993**, *98*, 5648-5652.
- (55) Hehre, W. J.; Ditchfield, R.; Pople, J. A. *J. Chem. Phys.* **1972**, *56*, 2257-2261.
- (56) Hay, P. J.; Wadt, W. R. *J. Chem. Phys.* **1985**, *82*, 299-310.
- (57) Berners-Price, S. J.; Ronconi, L.; Sadler, P. J. *Prog. Nucl. Magn. Reson. Spectrosc.* **2006**, *49*, 65-98.
- (58) Pregosin, P. S. *Coord. Chem. Rev.* **1982**, *44*, 247-291.
- (59) Still, B. M.; Kumar, P. G. A.; Aldrich-Wright, J. R.; Price, W. S. *Chem. Soc. Rev.* **2007**, *36*, 665-686.
- (60) Cohen, S. M.; Brown, T. H. *J. Chem. Phys.* **1974**, *61*, 2985-2986.
- (61) Gummin, D. D.; Ratilla, E. M. A.; Kostić, N. M. *Inorg. Chem.* **1986**, *25*, 2429-2433.
- (62) Galbraith, J. A.; Menzel, K. A.; Ratilla, E. M. A.; Kostić, N. M. *Inorg. Chem.* **1987**, *26*, 2073-2078.
- (63) Norman, R. E.; Ranford, J. D.; Sadler, P. J. *Inorg. Chem.* **1992**, *31*, 877-888.
- (64) Scaffidi-Domianello, Y. Y.; Meelich, K.; Jakupec, M. A.; Arion, V. B.; Kukushkin, V. Y.; Galanski, M.; Keppler, B. K. *Inorg. Chem.* **2010**, *49*, 5669-5678.
- (65) Dolman, R. C.; Deacon, G. B.; Hambley, T. W. *J. Inorg. Biochem.* **2002**, *88*, 260-267.
- (66) Hall, M. D.; Amjadi, S.; Zhang, M.; Beale, P. J.; Hambley, T. W. *J. Inorg. Biochem.* **2004**, *98*, 1614-1624.
- (67) Beattie, J. K.; Starink, J. *Inorg. Chem.* **1975**, *14*, 996-999.
- (68) Gibson, D. *Dalton Trans.* **2009**, 10681-10689.

- (69) Nemirovski, A.; Vinograd, I.; Takroui, K.; Mijovilovich, A.; Rompel, A.; Gibson, D. *Chem. Commun.* **2010**, *46*, 1842-1844.

Table of Contents Synopsis:

A series of eight platinum(IV) complexes bearing axial carbamate ligands was synthesized. The physical properties of the complexes were investigated, and their cytotoxicity against two human cell lines was determined.

